Supporting Information for RocMLMs: Predicting Rock Properties through Machine Learning Models

Buchanan Kerswell [1] **Nestor Cerpa** [1] **Andréa Tommasi** [1] **Marguerite Godard** [1] **José Alberto Padrón-Navarta** [2]

[1]Géosciences Montpellier, Université de Montpellier & CNRS, Montpellier, France

[2]Instituto Andaluz de Ciencias de la Tierra, CSIC–UGR, Granada, Spain

Contents of this File

1. Figures S1 to S6
2. Tables S1

Corresponding author: Buchanan Kerswell, buchanan.kerswell@umontpellier.fr

Synthetic Peridotite Compositions

Figure S1 shows a comparison between natural peridotite compositions in the standardized Earthchem.org dataset and synthetic peridotite compositions sampled randomly along the PCA mixing array as described in Section 2.1.2 of the main text. The data in Figure S1 are the same as presented in Figure 2 of the main text, but show peridotite compositions in chemical space (Harker diagrams vs. SiO_2) instead of PC space. The trend from more fertile lherzolite samples to more depleted harzburgite samples is closely approximated by the synthetic peridotite mixing array. While PUM and DMM are often represented in the literature as distinct mantle end-members, they have quite similar major oxide compositions (e.g., Al_2O_3, CaO, MgO, and FeO). Synthetic mantle end-members PSUM and DSUM represent a much wider range of recorded mantle compositions than PUM and DMM (Figure S1).

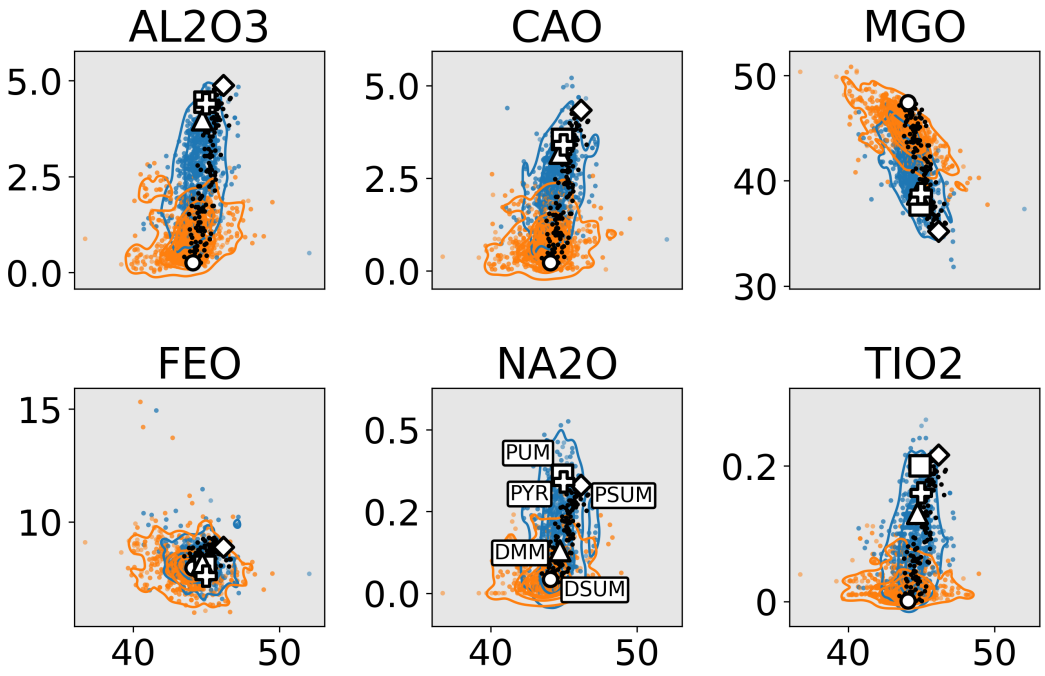

Figure S1: Harker Diagrams vs. SIO2 (in wt.%) showing the distribution of peridotite samples from Earthchem.org (colored data points and contours). PUM (white square), DMM (white triangle), and pyrolite (white plus) are commonly-referenced bulk mantle compositions (see Table 2 in the main text), while PSUM (white diamond) and DSUM (white circle) define a mixing array used to generate RocMLM training data (black data points).

RocMLM Regression Algorithms

Figures S2–S6 show RocMLM predictions and depth profiles for a PUM bulk mantle composition. The Decision Tree, single-layer Neural Network, and three-layer Neural Network RocMLMs were presented in the main text (Figures 3–5), while the k-Neighbors (Figure S3) and two-layer Neural Network RocMLMs (Figures S5) are presented here for a comprehensive comparison of all the regression algorithms tested in this study.

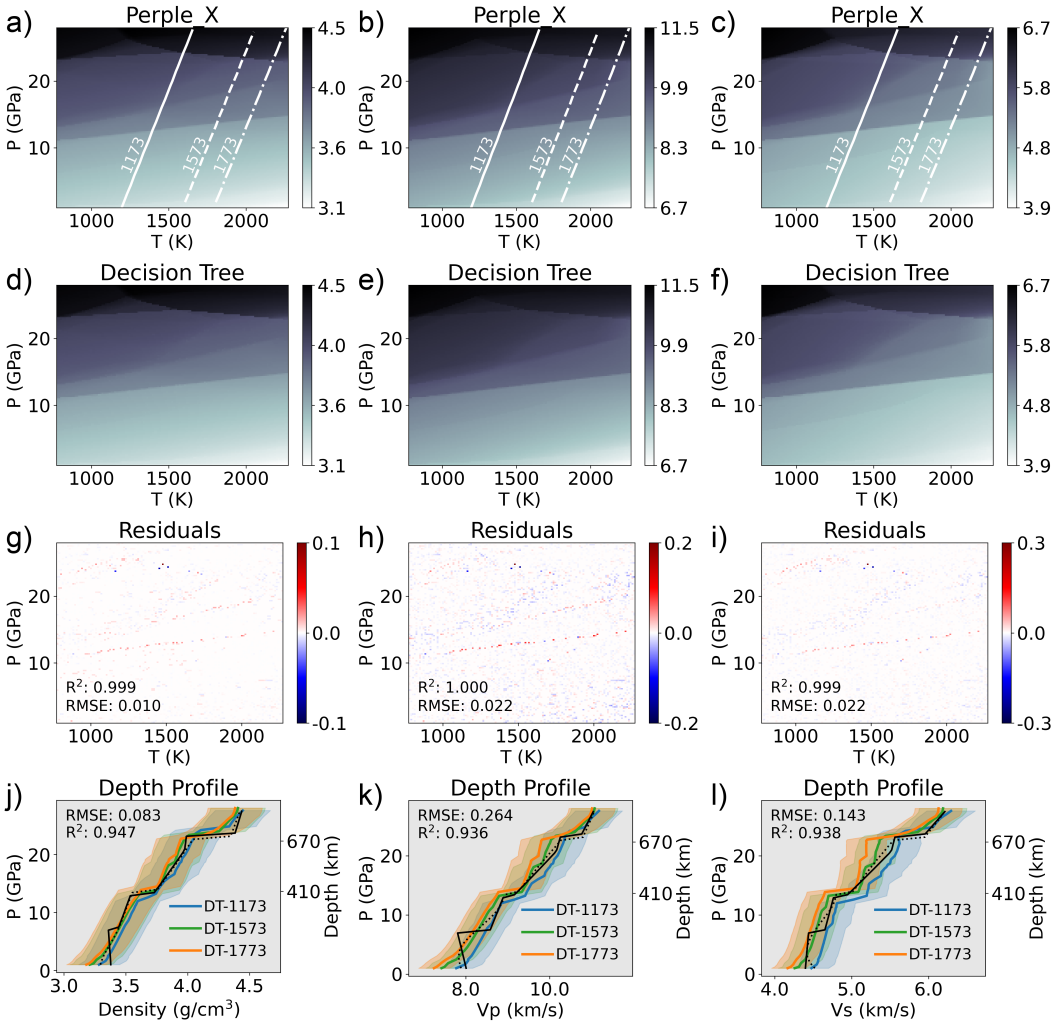

Figure S2: (ref:image12-PUM-DT-cap)

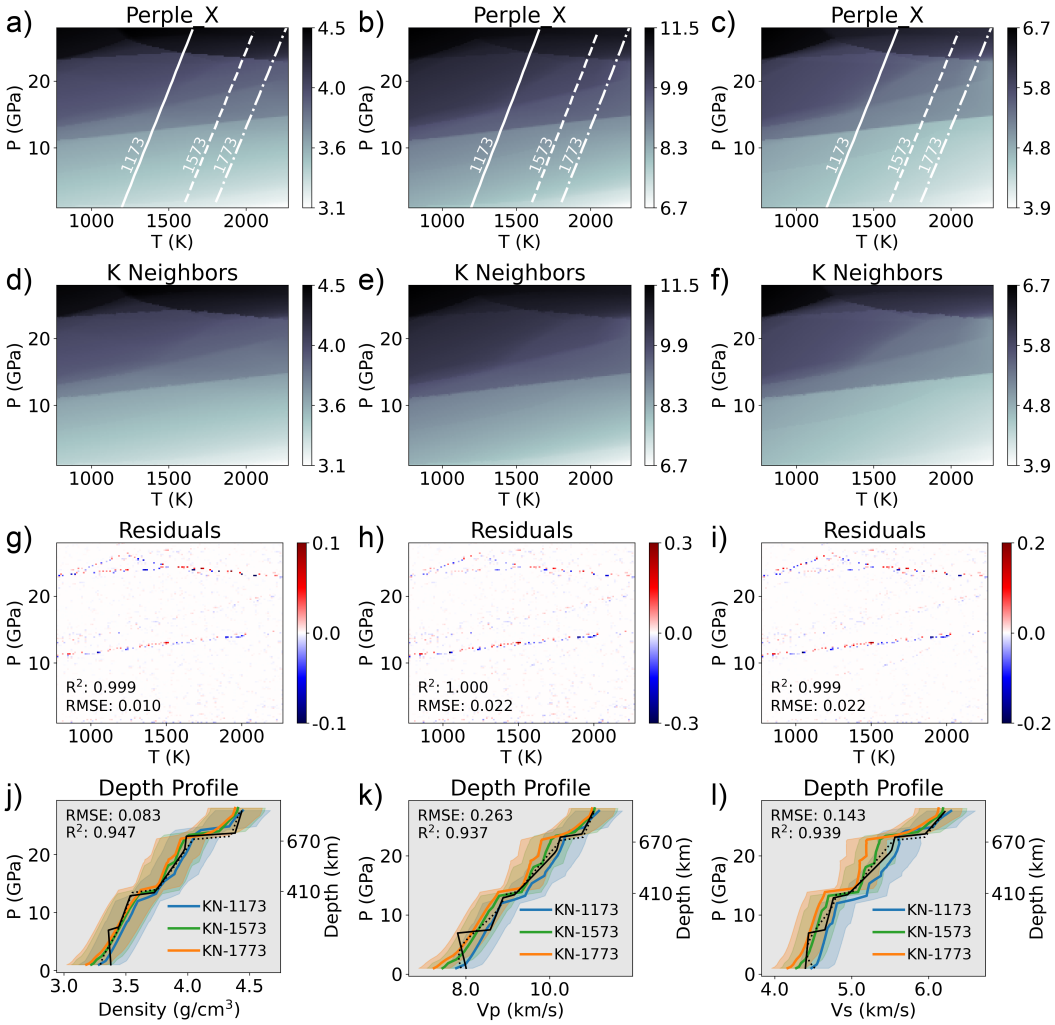

Figure S3: (ref:image12-PUM-KN-cap)

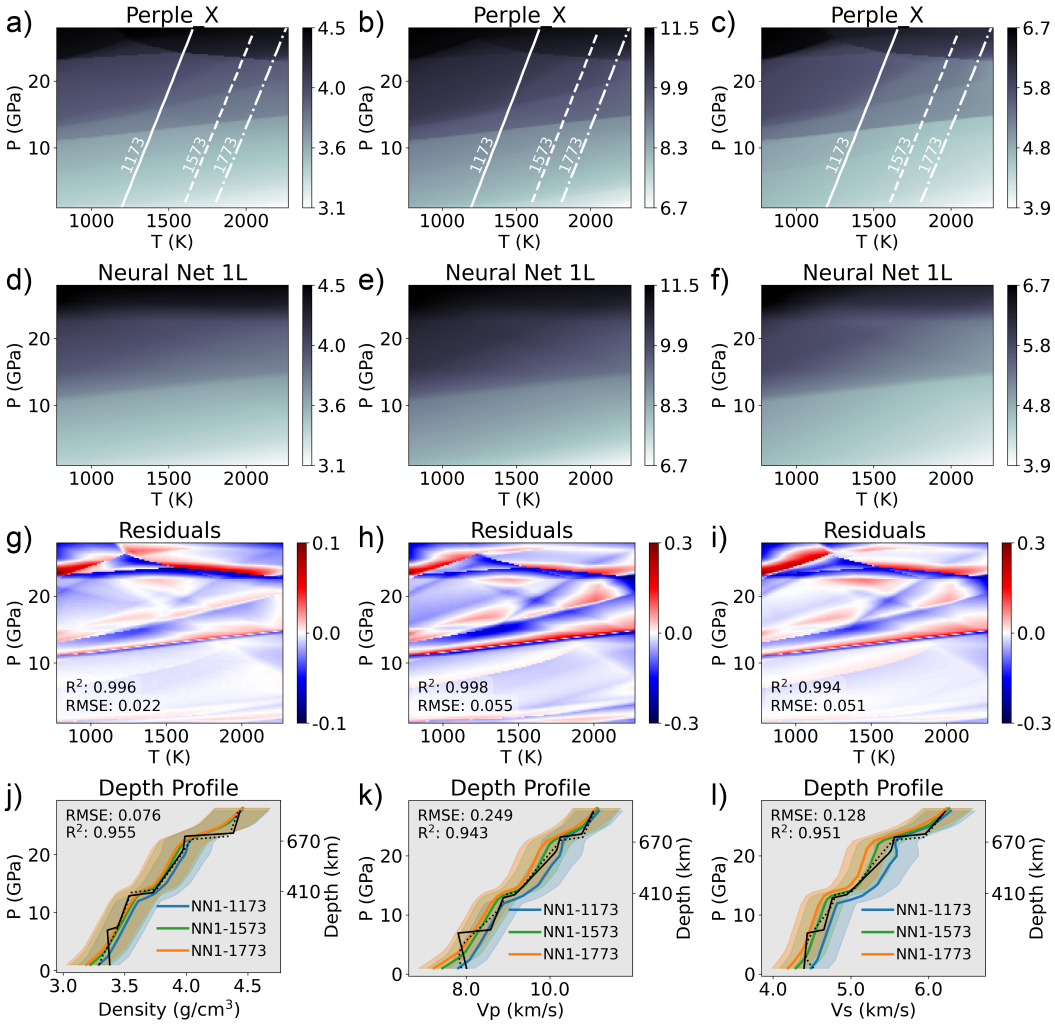

Figure S4: (ref:image12-PUM-NN1-cap)

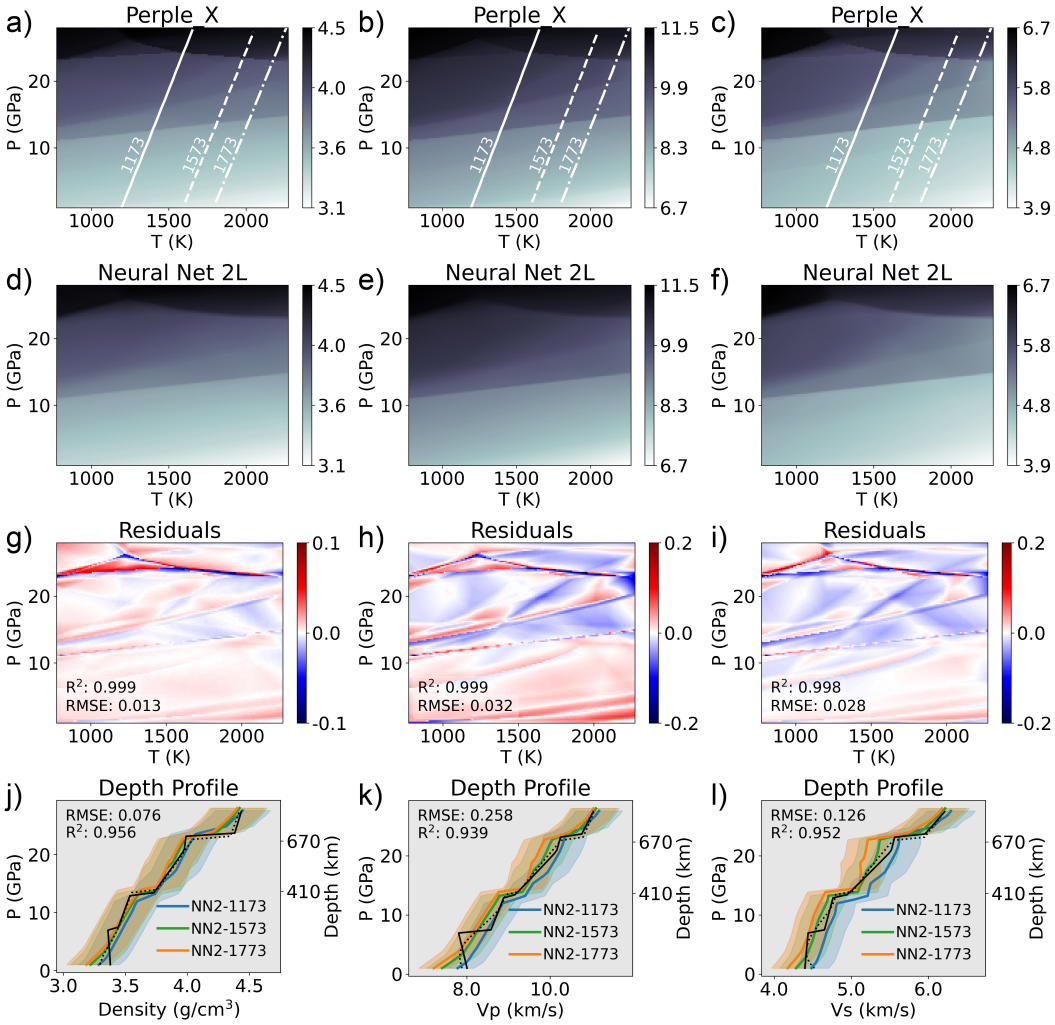

Figure S5: (ref:image12-PUM-NN2-cap)

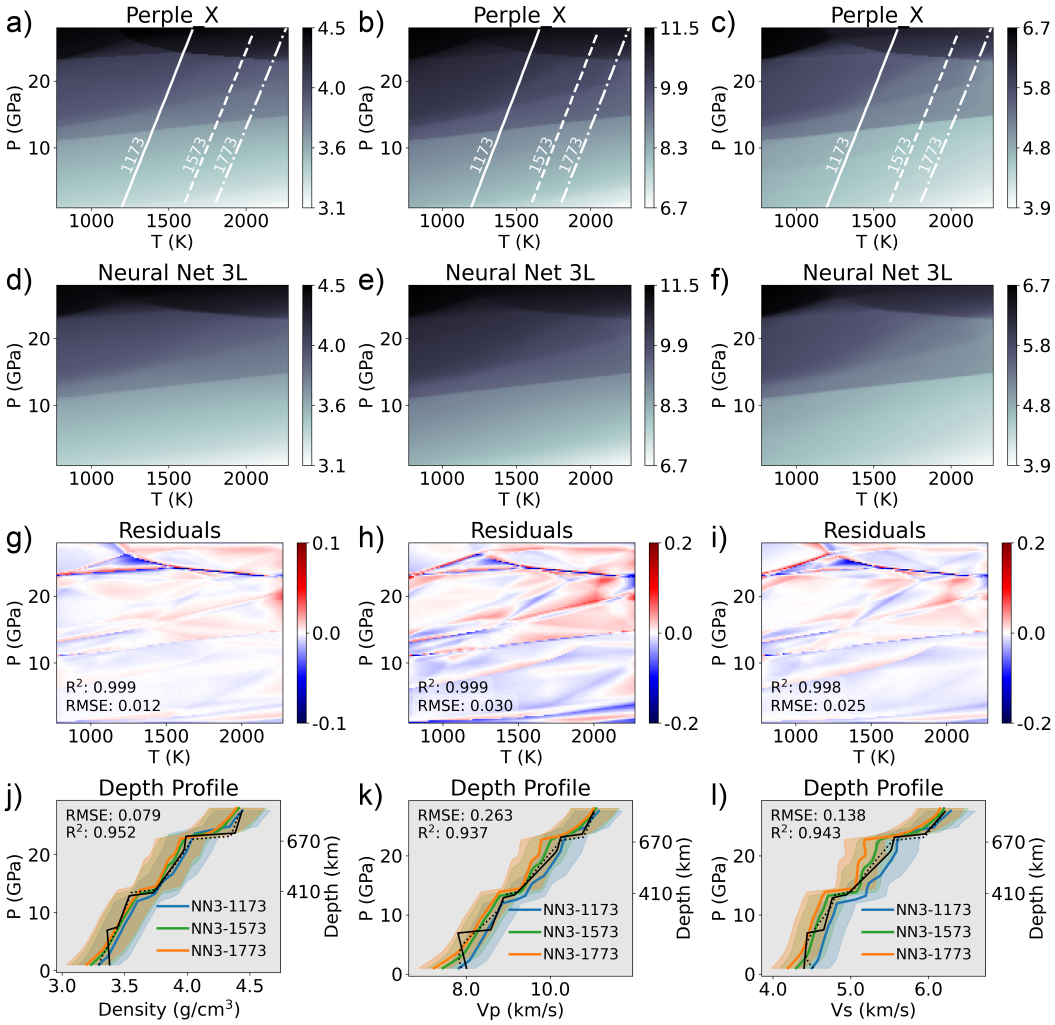

Figure S6: (ref:image12-PUM-NN3-cap)

GFEM, Lookup Table, and RocMLM Performance Datasets

The Lookup Table and GFEM performance data referenced in the main text are not included here for brevity, but can be found at `https://doi.org/10.17605/OSF.IO/K23TB`. These data are shown in Figure 6 of the main text and referenced in the Introduction of the main text to give a sense of the execution speeds of widely-used GFEM programs (4–228 ms per PTX point). The Introduction of the main text also references a feasibility objective for RocMLM performance (10^0–10^{-1} ms), which was estimated with the following reasoning. Numerical geodynamic models on the order of 2000 x 300 km in scale, containing at least 277,221 nodes (921 x 301, e.g., Kerswell et al., 2021) are widely-considered "high-resolution". Running GFEM on each node (at 4–228 ms/node) would take between 18.5 minutes to 17.5 hours with modern GFEM programs, depending on their configuration and assuming a simple sequential computation. At execution speeds of 10^0–10^{-1} ms, however, only 0.5–4.5 minutes of computation time would be added to each timestep, in a similar context. We consider an additional 0.5–4.5 minutes per timestep reasonable considering the advantage of implementing thermodynamic self-consistency in numerical experiments, especially given that parallel computing would further decrease these time estimations. We therefore set 10^0–10^{-1} ms as a minimum feasibility objective for RocMLM execution speeds.

Note that Figure 6 of the main text shows a representative subset of the RocMLM performance data evaluated in this study. RocMLM performance was measured multiple times for each regression algorithm: iterating over all combinations of PT and X resolutions (Table S1), or model "capacities", which was too much data to include in the main text. For graphical clarity, Figure 6 of the main text only shows the set of RocMLM models with the lowest prediction times for each unique model capacity (ranging from 2^{11}–2^{21}). The same filtering procedure is equally applied to Lookup Table results. Removing this filtering step (or alternatively selecting for the highest prediction times) does not alter the main conclusions discussed in Section 4 of the main text, but does make the results presented in Figure 6 of the main text easier to digest for the reader. For transparency and reproducibility, the complete RocMLM performance dataset is contained in Table S1 below.

Table S1: RocMLM PTX resolution, accuracy (RMSE vs. Perple_X), and performance (training and prediction times) measured on a validation dataset after training.

Model	PT Res (pts)	X Res (pts)	Train (ms)	Predict (ms)	RMSE rho (g/cm^3)	RMSE Vp (km/s)	RMSE Vs (km/s)	Filesize (Mb)
DT	8	2	0.77	0.03	0.017	0.038	0.038	0.034
DT	8	32	2.8	0.04	0.014	0.034	0.034	0.313
DT	8	64	5.1	0.05	0.014	0.034	0.034	0.572
DT	8	128	8.5	0.05	0.014	0.034	0.034	0.52
DT	16	2	1.1	0.04	0.0098	0.022	0.021	0.117
DT	16	32	9.7	0.04	0.013	0.029	0.027	1.12
DT	16	64	19	0.05	0.013	0.029	0.027	2.04
DT	16	128	34	0.05	0.014	0.029	0.027	1.86
DT	32	2	3.6	0.04	0.0099	0.022	0.02	0.44
DT	32	32	43	0.07	0.011	0.022	0.021	4.22
DT	32	64	39	0.07	0.011	0.022	0.022	4.63
DT	32	128	170	0.09	0.011	0.022	0.022	7.02
DT	64	2	14	0.04	0.011	0.022	0.022	1.7
DT	64	32	220	0.09	0.011	0.023	0.022	16.4
DT	64	64	440	0.11	0.012	0.023	0.022	29.8
DT	64	128	790	0.15	0.012	0.023	0.023	27.2
DT	128	2	64	0.06	0.01	0.022	0.022	6.71
DT	128	32	1000	0.12	0.011	0.023	0.022	64.4
DT	128	64	2100	0.17	0.011	0.023	0.022	117
DT	128	128	4100	0.18	0.011	0.023	0.022	108
KN	8	2	0.39	0.18	0.027	0.078	0.058	0.017
KN	8	32	0.61	0.16	0.015	0.035	0.034	0.174
KN	8	64	0.98	0.16	0.015	0.035	0.034	0.342
KN	8	128	1.6	0.17	0.015	0.034	0.034	0.678
KN	16	2	0.47	0.14	0.015	0.041	0.033	0.057
KN	16	32	1.5	0.17	0.014	0.031	0.028	0.603
KN	16	64	2.9	0.18	0.014	0.029	0.027	1.19

Model	PT Res (pts)	X Res (pts)	Train (ms)	Predict (ms)	RMSE rho (g/cm^3)	RMSE Vp (km/s)	RMSE Vs (km/s)	Filesize (Mb)
KN	16	128	6	0.23	0.014	0.029	0.027	2.35
KN	32	2	0.67	0.22	0.011	0.028	0.024	0.21
KN	32	32	7.4	0.45	0.011	0.024	0.023	2.27
KN	32	64	14	0.29	0.011	0.023	0.022	4.48
KN	32	128	31	0.31	0.011	0.023	0.022	8.89
KN	64	2	2.1	0.21	0.011	0.023	0.022	0.814
KN	64	32	29	0.3	0.012	0.024	0.023	8.82
KN	64	64	56	0.33	0.012	0.023	0.023	17.4
KN	64	128	120	0.35	0.012	0.023	0.023	34.5
KN	128	2	8.4	0.2	0.01	0.022	0.022	3.2
KN	128	32	130	0.47	0.011	0.023	0.022	34.8
KN	128	64	270	0.62	0.011	0.023	0.022	68.5
KN	128	128	610	0.95	0.011	0.023	0.022	136
NN1	8	2	240	0.03	0.049	0.15	0.12	0.02
NN1	8	32	450	0.04	0.042	0.13	0.11	0.02
NN1	8	64	13000	0.1	0.04	0.12	0.096	0.02
NN1	8	128	14000	0.09	0.035	0.09	0.077	0.02
NN1	16	2	270	0.04	0.052	0.15	0.13	0.02
NN1	16	32	14000	0.13	0.036	0.087	0.081	0.02
NN1	16	64	16000	0.12	0.029	0.072	0.068	0.02
NN1	16	128	32000	0.1	0.021	0.06	0.055	0.02
NN1	32	2	14000	0.07	0.04	0.12	0.099	0.02
NN1	32	32	32000	0.13	0.025	0.061	0.057	0.02
NN1	32	64	51000	0.11	0.022	0.055	0.051	0.02
NN1	32	128	82000	0.16	0.019	0.05	0.046	0.02
NN1	64	2	15000	0.08	0.03	0.073	0.068	0.019
NN1	64	32	84000	0.13	0.02	0.048	0.044	0.019
NN1	64	64	140000	0.11	0.016	0.039	0.039	0.019
NN1	64	128	250000	0.14	0.017	0.045	0.041	0.019
NN1	128	2	36000	0.12	0.022	0.055	0.051	0.02

Model	PT Res (pts)	X Res (pts)	Train (ms)	Predict (ms)	RMSE rho (g/cm^3)	RMSE Vp (km/s)	RMSE Vs (km/s)	Filesize (Mb)
NN1	128	32	250000	0.1	0.017	0.041	0.038	0.02
NN1	128	64	500000	0.13	0.017	0.042	0.04	0.02
NN1	128	128	980000	0.11	0.016	0.039	0.036	0.02
NN2	8	2	290	0.04	0.045	0.12	0.11	0.045
NN2	8	32	14000	0.07	0.034	0.098	0.089	0.045
NN2	8	64	26000	0.13	0.024	0.076	0.072	0.045
NN2	8	128	28000	0.11	0.016	0.046	0.04	0.045
NN2	16	2	14000	0.1	0.046	0.12	0.11	0.045
NN2	16	32	28000	0.1	0.017	0.056	0.046	0.045
NN2	16	64	32000	0.09	0.015	0.043	0.035	0.045
NN2	16	128	63000	0.15	0.014	0.037	0.032	0.045
NN2	32	2	26000	0.11	0.033	0.088	0.079	0.045
NN2	32	32	63000	0.11	0.013	0.032	0.027	0.045
NN2	32	64	96000	0.12	0.012	0.032	0.027	0.045
NN2	32	128	150000	0.14	0.013	0.037	0.033	0.045
NN2	64	2	29000	0.13	0.02	0.054	0.048	0.043
NN2	64	32	160000	0.18	0.013	0.032	0.029	0.043
NN2	64	64	270000	0.15	0.011	0.03	0.026	0.043
NN2	64	128	500000	0.16	0.012	0.031	0.028	0.043
NN2	128	2	67000	0.16	0.013	0.032	0.028	0.045
NN2	128	32	510000	0.15	0.012	0.028	0.025	0.045
NN2	128	64	1e+06	0.14	0.015	0.032	0.03	0.045
NN2	128	128	2.1e+06	0.19	0.015	0.037	0.032	0.045
NN3	8	2	330	0.04	0.04	0.12	0.1	0.069
NN3	8	32	27000	0.1	0.021	0.061	0.059	0.069
NN3	8	64	40000	0.11	0.016	0.048	0.044	0.069
NN3	8	128	42000	0.15	0.016	0.042	0.037	0.069
NN3	16	2	27000	0.08	0.04	0.12	0.099	0.069
NN3	16	32	42000	0.16	0.015	0.048	0.039	0.069
NN3	16	64	47000	0.11	0.015	0.042	0.035	0.069

Model	PT Res (pts)	X Res (pts)	Train (ms)	Predict (ms)	RMSE rho (g/cm^3)	RMSE Vp (km/s)	RMSE Vs (km/s)	Filesize (Mb)
NN3	16	128	91000	0.16	0.016	0.041	0.034	0.069
NN3	32	2	40000	0.2	0.028	0.072	0.067	0.069
NN3	32	32	92000	0.13	0.011	0.027	0.024	0.069
NN3	32	64	140000	0.13	0.014	0.037	0.033	0.069
NN3	32	128	220000	0.13	0.012	0.03	0.026	0.069
NN3	64	2	44000	0.14	0.016	0.044	0.037	0.068
NN3	64	32	230000	0.17	0.013	0.028	0.026	0.068
NN3	64	64	400000	0.14	0.012	0.027	0.025	0.068
NN3	64	128	780000	0.18	0.012	0.027	0.024	0.068
NN3	128	2	97000	0.18	0.012	0.03	0.025	0.069
NN3	128	32	780000	0.15	0.011	0.025	0.023	0.069
NN3	128	64	1.6e+06	0.12	0.011	0.025	0.023	0.069
NN3	128	128	2.9e+06	0.16	0.012	0.025	0.024	0.069

1 References

References

Kerswell, B., Kohn, M., and Gerya, T. (2021). Backarc lithospheric thickness and serpentine stability control slab-mantle coupling depths in subduction zones. *Geochemistry, Geophysics, Geosystems*, 22(6):e2020GC009304.